Geophysical Research Letters

RESEARCH LETTER
10.1029/2021GL096740

Key Points:

- Spray droplet production by collective bursting bubbles is non-monotonic as surfactant concentration increases
- An optimal drop production is observed at intermediate surfactant concentrations for short-lived, non-coalescing surface bubbles
- The saturation of the water surface by air bubbles, or formation of a foam, inhibits the drop production by bubble bursting

Supporting Information:

Supporting Information may be found in the online version of this article.

Correspondence to:

L. Deike,
ldeike@princeton.edu

Citation:

Néel, B., Erinin, M. A., & Deike, L. (2022). Role of contamination in optimal droplet production by collective bubble bursting. *Geophysical Research Letters*, *49*, e2021GL096740. https://doi.org/10.1029/2021GL096740

Received 22 OCT 2021
Accepted 15 DEC 2021

Author Contributions:

Conceptualization: B. Néel, L. Deike
Data curation: B. Néel, M. A. Erinin
Formal analysis: B. Néel
Funding acquisition: L. Deike
Supervision: L. Deike
Writing – original draft: B. Néel, L. Deike
Writing – review & editing: B. Néel, M. A. Erinin, L. Deike

© 2021. American Geophysical Union. All Rights Reserved.

Role of Contamination in Optimal Droplet Production by Collective Bubble Bursting

B. Néel[1], M. A. Erinin[1], and L. Deike[1,2]

[1]Department of Mechanical & Aerospace Engineering, Princeton University, Princeton, NJ, USA, [2]High Meadows Environmental Institute, Princeton University, Princeton, NJ, USA

Abstract Gas bubbles bursting at the sea surface produce drops, which contribute to marine aerosols. The contamination or enrichment of water by surface-active agents, of biological or anthropogenic origin, has long been recognized as affecting the bubble bursting processes and the spray composition. However, despite an improved understanding of the physics of a single bursting event, a quantitative understanding of the role of the physico-chemical conditions on assemblies of bursting bubbles remains elusive. We present experiments on the drop production by millimetric, collective bursting bubbles, under varying surfactant concentration and bubble density. We demonstrate that the production of supermicron droplets (with radius larger than 35 μm) is non-monotonic as the surfactant concentration increases. The bursting efficiency is optimal for short-lived, sparsely distributed and non-coalescing bubbles. We identify the combined role of contamination on the surface bubble arrangement and the modification of the jet drop production process in the bursting efficiency.

Plain Language Summary Understanding the production of primary ocean spray aerosol and its dependence on meteorological and environmental variables is critical for modeling potentially health-adverse effects from dispersants used to break down oil spills, as well as radiative processes and cloud microphysical properties. We demonstrate experimentally that the coupling between the chemical properties of contaminated water and the physical mechanism of droplet production when a bubble bursts controls the efficiency of aerosols production during collective bubble bursting, and reveals an optimal production regime at intermediate contamination. This fundamental study paves the way to improved predictions of aerosol production in contaminated water.

1. Introduction

A gas bubble sitting at the surface of water ends its life in a burst. When it pops, it may eject drops, according to two mechanisms: the cap film puncturing, retraction and destabilization into a mist of film drops (Blanchard, 1963; Lhuissier & Villermaux, 2012), or the later collapse of the cavity into a vertical upwards jet that destabilizes into jet drops (Brasz et al., 2018; Duchemin et al., 2002; Ghabache et al., 2014; Ghabache & Séon, 2016; Spiel, 1994, 1997; Woodcock et al., 1953). These two production mechanisms have been extensively studied and documented for single bubbles, leading to various scalings laws to describe the mean size, distribution and number of ejected film (Lhuissier & Villermaux, 2012) and jet drops (Berny et al., 2021; Deike et al., 2018; Gañán-Calvo, 2017; Gañán-Calvo & López-Herrera, 2021; Gordillo & Rodríguez-Rodríguez, 2019; Lai et al., 2018) as a function of the controlling non-dimensional length scales $R_b/l_\mu = La$ (Laplace number) and $R_b/l_c = \sqrt{Bo}$ (Bo is the Bond number), with R_b the bubble size, $l_\mu = \mu^2/\gamma\rho$ the visco-capillary length, $l_c = \sqrt{\gamma/\rho g}$ the gravity-capillary length, μ and ρ the liquid viscosity and density, γ the surface tension and g gravity.

These scaling laws derived from a single bursting event can in principle be extrapolated to the production of droplets in a marine environment, using estimations of the number of bubbles at the ocean surface through the whitecap coverage method or the breaking wave distribution (Deike, 2022; Lewis & Schwartz, 2004; Veron, 2015). However, large uncertainties remain due to the wide range of scales involved as well as an incomplete understanding of the collective behavior of bubbles at the water surface (Modini et al., 2013; Néel & Deike, 2021; Sellegri et al., 2006) and the complex role of water contamination on individual bursting processes (Constante-Amores et al., 2021; Poulain et al., 2018). Therefore, a physical description of the collective bursting of bubbles in contaminated water is necessary, since it controls the formation, stability, and decay of foams on the ocean surface (Garrett, 1967; Peltzer & Griffin, 1987). Implications are far reaching, from remote sensing of the ocean surface (Callaghan et al., 2017), which is central to the study of marine aerosols, sources of cloud condensation nuclei

and light scattering particles, production from bursting bubbles (Lewis & Schwartz, 2004; Wang et al., 2017); as well as to better understand the generation and composition of aerosols associated with chemical agents used in oil-spill mitigation (Afshar-Mohajer et al., 2018; Feng et al., 2014; Sampath et al., 2019).

The seemingly basic question: "do bubbles burst collectively the same way as they burst individually?" often assumed in existing models, remains unanswered. Although the physico-chemical properties of water have long been identified in modulating the droplet production and final sea spray aerosol composition (Cochran et al., 2017; Collins et al., 2014; Sellegri et al., 2006; Wang et al., 2017), its precise effects on the surface bubbles assembly, or the drops production mechanisms remain poorly understood in the context of large bubbles rafts (Néel & Deike, 2021). Various experimental studies have attempted to quantify the role of water contamination by surfactant, biological activity or seawater temperature, and have yielded results sometimes contradicting each other (Frossard et al., 2019; Modini et al., 2013; Prather et al., 2013). The trends of production efficiency with contamination for assemblies of bubbles drifting at the surface, directly observed in laboratory experiments mimicking field conditions (Prather et al., 2013), produced from bubbling device in seawater (Frossard et al., 2019; Sellegri et al., 2006), or simulated in the laboratory from breaking waves experiments (Modini et al., 2013), remain unclear.

Here we present the results of a laboratory experiment which studies the spray production by collective bubble bursting at the surface of water, contaminated by surfactant. The experiment is designed to (a) produce narrow, normal distributions of millimetric bubbles in the bulk, (b) observe the arrangement and collective dynamics and statistics of the bubbles at the water surface, and (c) measure the drop production directly, immediately above the water surface. We control the water surface contamination by minute additions of surfactants Triton X-100 and sodium dodecyl sulfate (SDS). This follows our work quantifying how the surface bubble size distribution and raft dynamics depends on the surfactant concentration and the rate of bubbles arriving at the water surface (Néel & Deike, 2021).

The existence of an optimal drop production with respect to contamination, a key finding of this study, is illustrated in §2. §3 investigates the statistics of the drop production, in direct correlation with the surface bubbles assembly. §4 generalizes by comparing the bursting efficiency of two surfactants, and §5 discusses the mechanisms of drop production.

2. Contamination Controlled Optimal Production

Bubbles are produced at the bottom of transparent acrylic tank by way of 16–48 needles (inner diameter 203 or 305 μm) connected to a pressurized air chamber and arranged on a ring, and producing each a regular stream of quasi-monodisperse, millimetric bubbles. They are visualized and detected in the bulk of the tank, from the side, and characterized by their volume-equivalent radius R_b (Figure 1a). The tank, with dimensions L60 × W60 × H25 cm^3, is open at the top, leaving the bubbles unconstrained once they reach the surface (Figure 1a). A top-down imaging allows for a direct measurement of their location and size, as illustrated in Figures 1b–1e and detailed in a recent study focusing on the surface bubble dynamics (Néel & Deike, 2021). Drops, produced by the bursting surface bubbles, are imaged and detected from the side by means of telecentric shadow imaging, which preserves the true drop size across the depth of field. The observation window, close to the surface, ensures that we measure the totality of the drop production. The drops are eventually characterized in a statistical way, for those with radius $r_d > 35$ μm (see Figures 1f–1i and technical details in Supporting Information S1).

Surface contamination is investigated by varying the surfactant concentration c of two surfactants (SDS and Triton X-100, from Sigma-Aldrich), in levels below, around and above the coalescence transition c_* (Oolman & Blanch, 1986; Yang & Maa, 1984), above which the merging of bubbles in contact is prevented by a shielding action from the surfactants ($c_* = 12$ μM for SDS, $c_* = 4$ μM for Triton X-100, as measured in Néel and Deike (2021)).

Figures 1b–1i illustrates how the surface contamination (top row) affects the droplet production (bottom row) as SDS concentration increases. It demonstrates visually that the knowledge of the bulk bubbles alone (size and production rate being unchanged) is not sufficient in order to predict the drops size and production rate. Figures 1b–1e (top row) shows representative instantaneous states of the bubbles at the surface. The concentrations of SDS we highlight (0, 16, 128 and 2,000 μM) span across the coalescence transition ($c_* = 12$ μM), and the surface

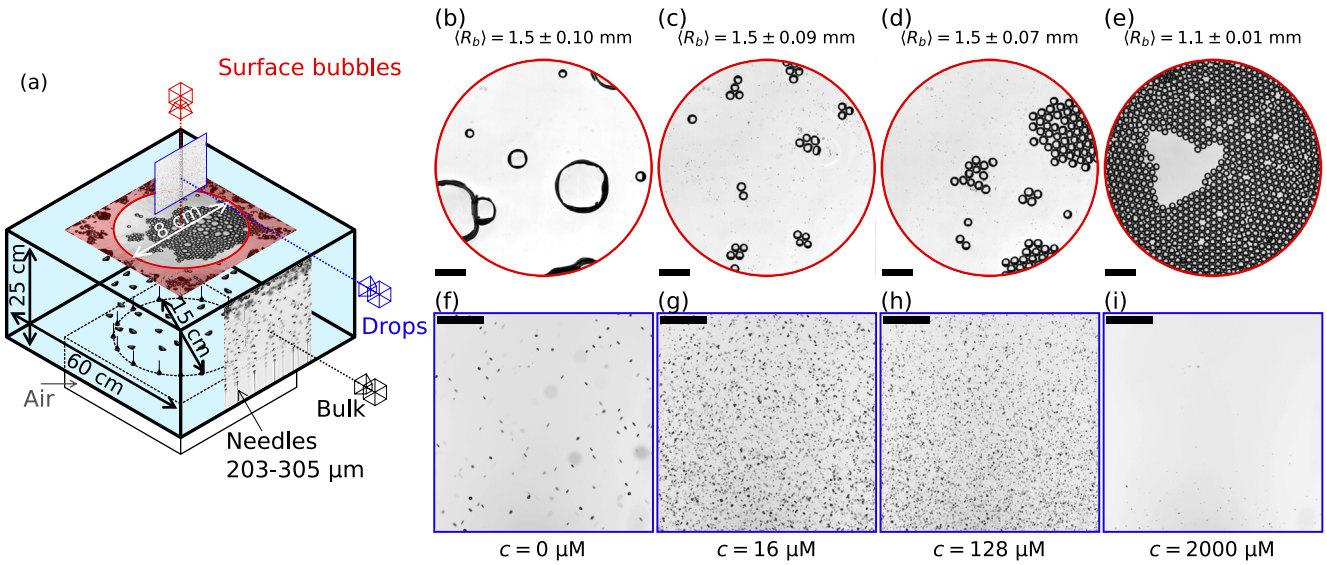

Figure 1. (a) Experimental setup: Bubbles are produced at the bottom of a transparent tank, then rise to the surface by buoyancy, where they are characterized from the top (red vignettes). Drops ejected by the bursting bubbles are imaged from the side (blue vignettes). (b–i) Surface bubbles and drops under identical bulk bubble production (bubbling rate $p_b = 830\,\mathrm{s}^1$, bubble mean radius $\langle R_b \rangle = 1.5 \pm 0.1$ mm), for increasing concentrations of SDS: $c = 0$, 16, 128 and 2,000 µM (left to right). (b–e) Typical instantaneous snapshots of the surface bubbles. (f–i) Time-integrated imaging of the spray production, for drops larger than 35 µm, seen from the side, 3.4 cm above the water surface (minimum of a stack of a 1,000 images acquired at 2 Hz, where drops appear in black on a white background). An optimal drop production is visible at intermediate contamination. Scale bars are 1 cm wide.

bubbles exhibit a large variety of arrangements, despite coming from identical gaussian bulk bubble populations. At low contamination (Figure 1b), surface bubbles merge and burst quickly, resulting in a small number of large, short-lived surface bubbles, typically 10^1 bubbles per cm^2 (see also Figure 3a below). At high contamination (Figure 1e), coalescence is prevented and bubbles form dense rafts drifting at the water surface, with surface densities reaching up to 10 bubbles per cm^2. In between, an intermediate regime (Figures 1c and 1d) is characterized by similar sized, short-lived bubbles that do not merge, assembling at most in small clusters before bursting, with between 0.1 and 1 bubbles per cm^2. This intermediate regime is due to the decoupled evolutions of the bubble merging and bursting rates with respect to the surfactant concentration, the coalescence transition occurring at a lower concentration than the onset of the stabilizing effect (Néel & Deike, 2021). The measured bursting and merging rates for these conditions are given in the Supporting Information S1 and Néel and Deike (2021).

Figures 1f–1i (bottom row) shows time-integrated images of the spray production corresponding to the four surface states shown in the top row of images. Very clearly, the drop production (in the detected range of radii $r_d > 35$ µm) is optimal in the intermediate regime where surface bubbles do not coalesce anymore, and form sparse rafts of few elements with relatively short life-times (Figures 1g and 1h). Many drops are ejected, with a wide size distribution. For a contamination below the coalescence transition $c < c_*$, fewer and larger bubbles are present at the surface, and less drops are produced in the $r_d > 35$ µm range (Figure 1f). Far above the concentration threshold $c \gg c_*$ (Figure 1i), the drops production decreases significantly, due to the increase in surface bubble lifetime, which leads to the formation of three-dimensional rafts.

3. Surface Transfer Function and Droplet Distribution

The number of spray drops and their size distribution is determined by the rearrangements of the bubbles on the surface. This surface arrangement controls the bubble sizes, their bursting mechanism (and their efficiency at producing drops), effectively acting as a surface transfer function. Figure 2 shows bulk bubble R_b, surface bubble R_s and drop r_d radius distributions, under identical bubbling conditions and increasing concentrations of SDS. It demonstrates the importance of considering the statistical details of the surface rearrangements: an identical normal distribution of bubbles in the bulk leads, under a varying surface contamination, to various size distributions of the surface bubbles and of the ejected drops.

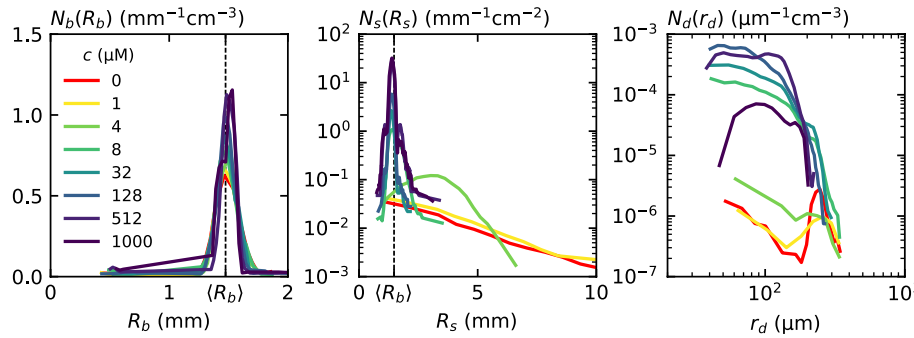

Figure 2. From monodisperse bulk bubble size distribution to drops production: a surface transfer function, under an increasing concentration of surfactant (SDSfrom 1 μM to 1 mM). (a) Bulk bubble distribution $N_b(R_b)$ is almost unchanged when increasing the contamination (colored lines), with mean diameter $\langle R_b \rangle = 1.5 \pm 0.1$ mm. (b) Surface bubble distribution $N_s(R_s)$, shifting from a broad distribution at low contamination when bubbles are able to coalesce to a narrower distribution close to $N_b(R_b)$ at high contamination. (c) Corresponding ejected drop distribution $N_d(r_d)$. The number and size of drops ejected evolve with the increased contamination and surface bubble distribution.

Figure 2a shows the bubble distribution in the bulk for the same bubbling conditions and increasing concentrations of surfactant SDS. The concentration is shown in colors and spans from $c = 0$ and 1 μM to $c = 1$ mM a fraction of the critical micellar concentration (CMC $c_{cm} = 8.2$ mM), crossing the coalescence transition $c_* = 12$ μM. The different bulk bubble size distributions $N_b(R_b)$ (for bubbles larger than $R_b > 400$ μm) all exhibit the same gaussian statistics, with a mean size $\langle R_b \rangle = 1.5$ mm which remain unchanged under a variation of the SDS concentration over three orders of magnitude: the addition of surfactant has no noticeable influence on the bubble production in the bulk.

Figure 2b shows the corresponding surface bubble size distributions $N_s(R_s)$. As the surfactant concentration c is increased, the surface distributions are modified in two ways. First, they narrow down around the bulk injection size $\langle R_b \rangle$, a direct consequence of the suppression of bubble coalescence events for concentrations $c > c_*$. Second, the magnitude of the distribution increases, with more bubbles populating the surface, a consequence of the increased stability, or lifetime, of the surface bubbles.

Figure 2c shows the drop size distribution $N_d(r_d)$, for drops in the range $r_d \geq 35$ μm. Deionized and barely contaminated water (red and yellow lines) produce two categories of drops. Above $r_d \geq 200$ μm, a narrow peak centered around $r_d = 250$ μm is immediately identified. For drops below $r_d \leq 200$ μm, the smaller the drops, the more of them are produced (down to the measurement cutoff $r_d = 35$ μm). The total number of drops produced at low contamination is lower than for higher surfactant concentrations, a consequence of the corresponding low surface bubbles density. When the surfactant concentration is increased to 4 μM of SDS (green line), the drop size distribution starts to transition, following the changes in the surface bubble population (Figure 2b). At this transition point, the total number of drops below $r_d < 200$ μm begins to increase with the concentration, with the peak initially around 250 μm gradually shifting to drop sizes close to 150 μm at the highest c. For SDS concentrations in the range $c = 10500$ μM, the drop size distributions are broader, and do not exhibit two distinct modes. For these concentrations, drops are produced in larger numbers, up to three orders of magnitude more when compared to the clean water case. When the surfactant concentration is increased further, above $c \geq 1$ mM of SDS, the number of drops decreases at all sizes $r_d > 35$ μm (dark blue line). This corresponds to a surface state where bubbles accumulate at the surface too quickly, when compared to their lifetime. They form large drifting rafts or even three-dimensional foams, which ultimately inhibit the drop ejection. Similar results are observed when using a different surfactant (Triton X-100) and for various bubble injection rates (see Supporting Information S1).

4. Bursting Efficiency and Mean Drop Size

We now relate the number of drops produced to the number of bubbles at the surface, as a function of the surface contamination. Figure 3a plots the surface bubble density $\rho_s = \int_{R_s} N_s(R_s) \mathrm{d}R_s$ (per unit area, black circles, left axis) and the drop density $\rho_d = \int_{r_d > 35\mu\mathrm{m}} N_d(r_d) \mathrm{d}r_d$ (per unit volume of air, green crosses, right axis) as a function of SDS concentration c, under the same bubbling conditions. As c is increased from 0 to $c \simeq 0.5$ mM, a fraction

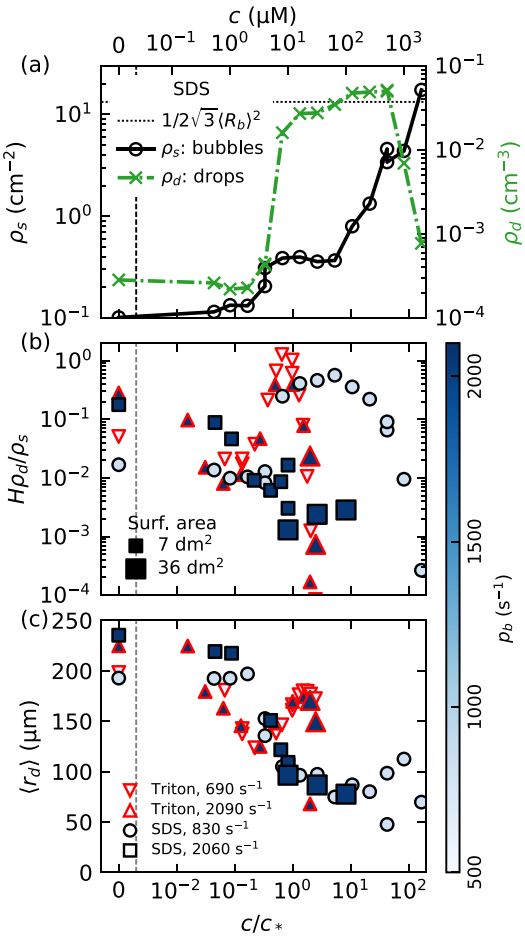

Figure 3. (a) Surface bubble density ρ_s (left axis, black circles) and drop density ρ_d (right axis, green crosses) as a function of the concentration c in SDS. (b) Bursting efficiency $\epsilon = H\rho_d/\rho_s$ ($H = 50$ mm) as a function of the normalized surfactant concentration c/c_* for Triton X-100 ($c_* = 4$ μM, red triangles) and SDS ($c_* = 12$ μM, black squares and circles). Two bubbling conditions are shown (p_b, color-coded in blue). (c) Mean drop radius $\langle r_d \rangle$ as a function of c/c_*.

of the CMC, both ρ_s and ρ_d increase. However, they do so at different rates: the surface bubble density ρ_s first undergoes an intermediate plateau around the coalescence transition $c_* = 12$ μM. Then ρ_s rises sharply to the maximal value $1/2\sqrt{3}\langle R_b \rangle^2$, the density of a close packing of disks with radius $\langle R_b \rangle$ where bubbles saturate the surface entirely. If the stability (lifetime) of the surface bubbles is increased even further for the same bubbling rate and total surface area available, they can start to pile up and form three-dimensional foams. For a given surfactant concentration the onset of foaming can be delayed in the experiment by providing a larger surface area over which bubbles can collect on, or changing the bubbling rate, as illustrated in the Supporting Information S1. In parallel to the evolution of ρ_s, the drop density ρ_d increases sharply between $c = 4$ and ≈ 10 μM followed by a more gradual increase until $c \approx 800$ μM. Next, when ρ_s saturates for $c \geq 800$ μM, the drop density ρ_d decreases abruptly, where the close packing of the bubbles, and the formation of a three-dimensional foam, inhibit the drops ejection.

We combine surface bubble density ρ_s and drop density ρ_d into a non-dimensional bursting efficiency $\epsilon = H\rho_d/\rho_s$, where H is a vertical height above the water surface where drops are measured (see Supporting Information S1). The bursting efficiency ϵ captures how different regimes of contamination affect drop ejection efficiency, under the same bulk bubble production, within the range of drop size measured ($r_d > 35$ μm). The bursting efficiency is plotted as a function of the surfactant concentration in Figure 3b, for two surfactants SDS and Triton X-100, with c normalized by c_*, the coalescence transition concentration ($c_* = 12$ μM for SDS, $c_* = 4$ μM for Triton X-100, Néel and Deike (2021)). The evolution of ϵ with respect to c/c_* exhibits similar features for both surfactants at low bubbling rate (light blue symbols): the efficiency first decreases as c increases before reaching a local maximum around $c \approx c_*$ (Triton X) to $c \approx 8c_*$ (for SDS). The efficiency decreases at high contamination corresponding to the transition to a three-dimensional foam. For a higher bubbling rate (dark blue symbols), the behavior for Triton X-100 is identical while for SDS, no local maxima is observed due to the occurence of packing at the surface at a lower concentration. This result indicates that while the overall behavior is similar for both surfactants, the range of optimal drop production is dependent on the type of surfactant, as well as the transition to packing at the surface. These dynamical features at the surface are themselves controlled by the interplay between the bubbling rate and the bubbles bursting and merging rates.

Figure 3c shows the mean drop radius $\langle r_d \rangle$ as a function of c/c_* for both SDS and Triton X-100. For SDS under two different bubble production rates, $\langle r_d \rangle$ continuously decreases with an increasing surfactant concentration, from $\langle r_d \rangle \approx 200$ μm for gently contaminated cases, to $\langle r_d \rangle \approx 70$ μm at high concentrations. In the case of Triton X-100, the mean drop size follows a similar trend as SDS until the coalescence concentration c_*, then reaches a very narrow local maximum around $c/c_* \approx 2$ when the bursting efficiency is the highest. Drop sizes thus seem to be only affected by the surfactant type and its concentration, as experiments performed under different bubbling rates exhibit the same trend.

5. Discussion and Production Models

We show in the previous sections and Néel and Deike (2021) that the ability of the surface bubbles to merge, form clusters and large rafts, pile up in three-dimensional foams, or burst isolated, depends on the interplay between surface contamination and bubble flux to the surface. The surface contamination, in particular, induces different collective effects on the bubbles (merging, or clustering), which in turn modifies the drop production, both in size and number. The evolution of the bursting efficiency as a function of the surfactant concentration highlights a complex behavior, with the existence of an optimal regime of production. We find that this optimal efficiency

occurs when bubbles burst in small rafts of few elements (see Figures 1b and 1c) sparsely distributed at the surface, suggesting that collective effects in large rafts tend to inhibit droplet production by bubble bursting. In turn, the effect of surfactants on the mean drop radius and total number distributions suggests a modification of the spray production mechanisms as the surface becomes more and more contaminated.

The production of drops from an assembly of surface bubbles can be analyzed within the framework proposed by Lhuissier and Villermaux (2012) for film drops and extended to jet drops by Berny et al. (2021), which integrates scalings for the number $n(R_s)$ and size of drops (mean size $\langle r_d \rangle(R_s)$ and distribution $p(r_d/\langle r_d \rangle, R_s)$) produced by a single bubble bursting over the distribution of bursting bubbles $N_s(R_s)$:

$$N_d(r_d) = \int_{R_s} \frac{N_s(R_s) n(R_s)}{\langle r_d \rangle (R_s)} p\left(\frac{r_d}{\langle r_d \rangle}, R_s\right) \mathrm{d}R_s \quad . \tag{1}$$

Figure 4 shows examples of the surface bubble distribution $N_s(R_s)$ in clean and contaminated regimes (Figure 4a) and the corresponding drop distribution $N_d(r_d)$ (Figure 4b), together with corresponding models associated with film drops (Lhuissier & Villermaux, 2012):

$$n(R_s) = \chi_F \left(\frac{R_s}{\ell_c}\right)^2 \left(\frac{R_s}{h_s}\right)^{7/8} \quad ; \quad \langle r_d \rangle = \eta_F R_s^{3/8} h_s^{5/8} \quad , \tag{2}$$

and jet drops (Berny et al., 2021):

$$n(R_s) = \chi_J \left(\frac{R_s}{\ell_\mu}\right)^{1/3} \quad ; \quad \langle r_d \rangle = \eta_J \ell_\mu \left(\frac{R_s}{\ell_\mu}\right)^{5/4} \quad . \tag{3}$$

h_s is the surface bubble cap film thickness, related to the bubble radius $h_s = R_s^2/\mathcal{L}$, with $\mathcal{L} \approx 20$ m (Lhuissier & Villermaux, 2012; Poulain et al., 2018). $\chi_{F,J}$ and $\eta_{F,J}$ are non-dimensional prefactors for the film (F) and jet (J) drop number and mean radius, respectively, and distributions $p(r_d/\langle r_d \rangle)$ are described by Gamma (Γ) distributions.

For clean water (red lines), surface bubbles are sorted into two categories: surface bubbles with sizes close to $\langle R_b \rangle = 1.5$ mm are known to produce between 1 and 3 jet drops when bursting in clean water (Berny et al., 2020; Ghabache & Séon, 2016; Spiel, 1994). This result is confirmed in our experiments by complementary dynamical observations shown in Figures 4c and 4e. The vertical upwards motion of the drops is consistent with the jet drop production mechanism (since the expected motion of film drops is mostly sideways). These jet drops explain the narrow peak around $\langle r_d \rangle = 250$ µm (Figure 4b solid red line), and are well described by the jet drop model (dotted red line) derived from single bubble bursting experiments (Berny et al., 2021; Gañán-Calvo, 2017; Lai et al., 2018). In the clean water case, larger bubbles in the exponentially-tailed surface distribution (Figure 4a dotted red line) are the result of at least one merging event. These bubbles are larger than the capillary length $R_s > l_c$ so that no jet drops are being produced when they burst. The resulting drops are assumed to be film drops, and the red dashed line shows the corresponding model derived from single bubble bursting experiments (Lhuissier & Villermaux, 2012). In both the jet (red dotted line) and film (red dashed line) models, we use the measured bubble surface distribution for R_s in the appropriate range of production. The agreement between the measured (Figure 4b solid red line) and predicted (dashed red line) distributions is good using the coefficients derived from single bursting experiments (Berny et al., 2021; Lhuissier & Villermaux, 2012).

For moderately contaminated water (blue line), surface bubbles do not coalesce and burst either isolated or in small rafts (Figures 1b, 1c and 4a). Their surface distribution is centered around $\langle R_b \rangle = 1.5$ mm, and they produce mostly jet drops (in the detected range, Figure 4b), as suggested by the upwards vertical motion of the ejected drops (Figures 4d and 4f). Unlike the clean water case, each bubble produces more and smaller drops, which are scattered in sizes, as illustrated in the representative sequence (Figure 4d). The drop size distribution can still be modeled by integration over the narrow surface bubbles distribution (Figure 4a dotted blue line) but now requires to modify the coefficients for the mean drop size and number of ejected drop, following the experimental results from Figures 3b and 3c, yielding the broad drop size distribution (Figure 4b dotted blue line).

The role of contamination and surface bubble rearrangement can be summarized as follow: A broad distribution of surface bubbles generates a narrow production of jet drops (in clean water), whereas a narrow distribution of

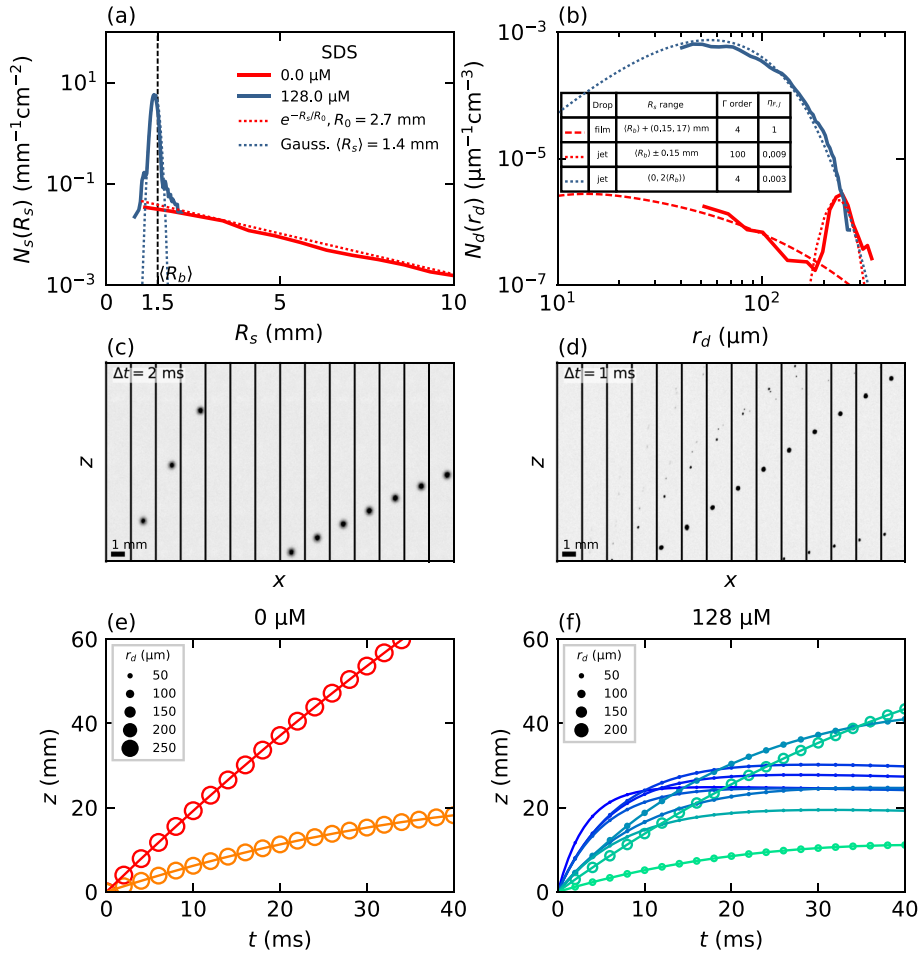

Figure 4. (a) Surface bubble radius $N_s(R_s)$ and (b) drop radius $N_d(r_d)$ distributions in deionized water (red lines) and contaminated water sodium dodecyl sulfate (SDS), $c = 128$ μM, blue lines, for bulk bubbles with mean radius $\langle R_b \rangle = 1.5$ mm. (a) Measured distributions are fitted by integrable functions (dotted lines). (b) Dashed and dotted lines are the integration by (1) of the corresponding surface bubble distributions, considering respectively a film drop or a jet drop mechanism. Integration parameters are given in the legend. (c and d) Image sequences highlighting the bursting of a single bubble (located below the frame), in (c) clean water (2 drops) and (d) with SDS at $c = 128$ μM (9 drops). Acquisition rates are respectively 500 and 1,000 Hz, scale bar is 1 mm wide. (e and f) Drop vertical trajectory $z(t)$ for the 2 bubble bursting shown in (c) and (d): (e) clean water (2 drops) and (f) with SDS at $c = 128$ μM (9 drops). Color indicates the drop ejection number (from darker colors for the first ejected drop to lighter color to the subsequent ones) and size of the symbols indicates the size of the drop.

surface bubbles leads to a jet drop distribution with a significantly broader dispersion (in contaminated water). Supported by the dynamical observations of Figures 4c–4f and the satisfactory comparison to a mechanistic model, this suggests that surfactants directly modify the bubble bursting mechanism: For contaminated water, more jet drops are being produced and of smaller sizes for the same original bubble. Furthermore, we note that the distribution amplitudes are orders of magnitude apart, linking back to the bursting efficiency previously defined: For bubble radii around $R_b \approx 1.5$ mm, the most efficient drop production mechanism seems to be jet drops. This jet drop mechanism is enhanced by the addition of surfactant which (a) prevents the coalescence of bubbles and stabilizes them, increasing their number at the surface, and (b) increases the number of drops generated by a bursting bubble while decreasing the average drop size. These two effects increase the bursting efficiency, until the formation of packed foams, which prevents drop production.

We show that even with a precisely controlled bubble production, the drop production differs greatly between different concentrations and types of surfactants. This results from collective re-arrangements of the bubbles at the surface (characterized by the merging and bursting rates) as well as a modification of the jet drop production

process, impacting both the size and number of ejected drops. Determining whether the influence of surfactants on the bursting processes results from collective effects or a modification of the individual jetting mechanism remains to be investigated. The resulting drop size distributions can be, and are, rationalized using the framework developed by Lhuissier and Villermaux (2012) and extended by Berny et al. (2021), but the knowledge of the surface transfer function and the changes in drop size and number being ejected for given contaminated conditions remain to be theoretically explained. The existence of an optimal production regime controlled by the interplay between the bubble production, bursting and merging rates could explain some of the apparent contradictions in the literature where these characteristics were unknown. Finally, while the present study focused on millimetric bubbles and drops above 30 μm, similar studies on smaller bubbles and drops, involving how the drop production might be affected by contamination and collective effects, may extend the present findings to sizes even more relevant to atmospheric applications, such as the origin for cloud condensation nuclei.

Data Availability Statement

Open research all data used in preparing this work are publicly available at https://doi.org/10.34770/pjmm-cp20.

Acknowledgments
This work has been supported by NSF Grant 1849762, and the Cooperative Institute for Earth System modeling between Princeton and the Geophysical Fluid Dynamics Laboratory (GFDL) NOAA. B. Néel and L. Deike designed research, performed research, analyzed data and wrote the paper; M. A. Erinin analyzed holography data presented in the Supporting Information S1. All authors edited the paper.

References

Afshar-Mohajer, N., Li, C., Rule, A. M., Katz, J., & Koehler, K. (2018). A laboratory study of particulate and gaseous emissions from crude oil and crude oil-dispersant contaminated seawater due to breaking waves. *Atmospheric Environment*, *179*, 177–186. https://doi.org/10.1016/j.atmosenv.2018.02.017

Berny, A., Deike, L., Séon, T., & Popinet, S. (2020). Role of all jet drops in mass transfer from bursting bubbles. *Physical Review Fluids*, *5*, 033605. https://doi.org/10.1103/physrevfluids.5.033605

Berny, A., Popinet, S., Séon, T., & Deike, L. (2021). Statistics of jet drop production. *Geophysical Research Letters*, *48*, e2021GL092919. https://doi.org/10.1029/2021GL092919

Blanchard, D. C. (1963). The electrification of the atmosphere by particles from bubbles in the sea. *Progress in Oceanography*, *1*, 73–202.

Brasz, C. F., Bartlett, C. T., Walls, P. L. L., Flynn, E. G., Yu, Y. E., & Bird, J. C. (2018). Minimum size for the top jet drop from a bursting bubble. *Physical Review Fluids*, *3*, 074001.

Callaghan, A. H., Deane, G. B., & Stokes, M. D. (2017). On the imprint of surfactant-driven stabilization of laboratory breaking wave foam with comparison to oceanic whitecaps. *Journal of Geophysical Research: Oceans*, *122*(8), 6110–6128. https://doi.org/10.1002/2017JC012809

Cochran, R. E., Ryder, O. S., Grassian, V. H., & Prather, K. A. (2017). Sea spray aerosol: The chemical link between the oceans, atmosphere, and climate. *Accounts of Chemical Research*, *50*(3), 599–604. https://doi.org/10.1021/acs.accounts.6b00603

Collins, D. B., Zhao, D. F., Ruppel, M. J., Laskina, O., Grandquist, J. R., Modini, R. L., & Prather, K. A. (2014). Direct aerosol chemical composition measurements to evaluate the physicochemical differences between controlled sea spray aerosol generation schemes. *Atmospheric Measurement Techniques*, *7*(11), 3667–3683. https://doi.org/10.5194/amt-7-3667-2014

Constante-Amores, C. R., Kahouadji, L., Batchvarov, A., Shin, S., Chergui, J., Juric, D., & Matar, O. K. (2021). Dynamics of a surfactant-laden bubble bursting through an interface. *Journal of Fluid Mechanics*, *911*. https://doi.org/10.1017/jfm.2020.1099

Deike, L. (2022). Mass transfer at the ocean-atmosphere interface: The role of wave breaking, droplets, and bubbles. *Annual Review of Fluid Mechanics*, *54*, 191–224. https://doi.org/10.1146/annurev-fluid-030121-014132

Deike, L., Ghabache, É., Liger-Belair, G., Das, A. K., Zaleski, S., Popinet, S., & Séon, T. (2018). Dynamics of jets produced by bursting bubbles. *Physical Review Fluids*, *3*, 013603. https://doi.org/10.1103/PhysRevFluids.3.013603

Duchemin, L., Popinet, S., Josserand, C., & Zaleski, S. (2002). Jet formation in bubbles bursting at a free surface. *Physical Fluids*, *14*(9), 3000–3008. https://doi.org/10.1063/1.1494072

Feng, J., Roché, M., Vigolo, D., Arnaudov, L. N., Stoyanov, S. D., Gurkov, T. D., & Stone, H. A. (2014). Nanoemulsions obtained via bubble-bursting at a compound interface. *Nature Physics*, *10*(8), 606–612. https://doi.org/10.1038/nphys3003

Frossard, A. A., Long, M. S., Keene, W. C., Duplessis, P., Kinsey, J. D., Maben, J. R., & Zhu, Y. (2019). Marine aerosol production via detrainment of bubble plumes generated in natural seawater with a forced-air venturi. *Journal of Geophysical Research: Atmospheres*, *124*(20), 10931–10950. https://doi.org/10.1029/2019JD030299

Gañán-Calvo, A. M. (2017). Revision of bubble bursting: Universal scaling laws of top jet drop size and speed. *Physical Review Letters*, *119*(20). https://doi.org/10.1103/PhysRevLett.119.204502

Gañán-Calvo, A. M. & López-Herrera, J. M. (2021). On the physics of transient ejection from bubble bursting. *Journal of Fluid Mechanics*, *929*. https://doi.org/10.1017/jfm.2021.791

Garrett, W. D. (1967). Stabilization of air bubbles at the air-sea interface by surface-active material. *Deep-Sea Research*, *14*(6), 661–672. https://doi.org/10.1016/S0011-7471(67)80004-4

Ghabache, É., Antkowiak, A., Josserand, C., & Séon, T. (2014). On the physics of fizziness: How bubble bursting controls droplets ejection. *Physical Fluids*, *26*, 121701. https://doi.org/10.1063/1.4902820

Ghabache, É. & Séon, T. (2016). Size of the top jet drop produced by bubble bursting. *Physical Review Fluids*, *1*(5). https://doi.org/10.1103/PhysRevFluids.1.051901

Gordillo, J. M. & Rodríguez-Rodríguez, J. (2019). Capillary waves control the ejection of bubble bursting jets. *Journal of Fluid Mechanics*, *867*, 556–571. https://doi.org/10.1017/jfm.2019.161

Lai, C.-Y., Eggers, J., & Deike, L. (2018). Bubble bursting: Universal cavity and jet profiles. *Physical Review Letters*, *121*, 144501. https://doi.org/10.1103/PhysRevLett.121.144501

Lewis, E. R. & Schwartz, S. E. (2004). *Sea salt aerosol production: Mechanisms, methods, measurements and models—A critical Review 152*. American Geophysical Union.

Lhuissier, H. & Villermaux, E. (2012). Bursting bubble aerosols. *Journal of Fluid Mechanics*, *696*, 5–44. https://doi.org/10.1017/jfm.2011.418

Modini, R. L., Russell, L. M., Deane, G. B., & Stokes, M. D. (2013). Effect of soluble surfactant on bubble persistence and bubble-produced aerosol particles. *Journal of Geophysical Research: Atmospheres*, *118*(3), 1388–1400. https://doi.org/10.1002/jgrd.50186

Néel, B. & Deike, L. (2021). Collective bursting of free-surface bubbles, and the role of surface contamination. *Journal of Fluid Mechanics*, *917*. https://doi.org/10.1017/jfm.2021.272

Oolman, T. O. & Blanch, H. W. (1986). Bubble coalescence in stagnant liquids. *Chemical Engineering Communications*, *43*(4–6), 237–261. https://doi.org/10.1080/00986448608911334

Peltzer, R. D. & Griffin, O. M. (1987). The stability and decay of foam in sea water. *Ocean Physics and Engineering*, *12*(2), 101–126.

Poulain, S., Villermaux, E., & Bourouiba, L. (2018). Ageing and burst of surface bubbles. *Journal of Fluid Mechanics*, *851*, 636–671. https://doi.org/10.1017/jfm.2018.471

Prather, K. A., Bertram, T. H., Grassian, V. H., Deane, G. B., Stokes, M. D., DeMott, P. J., & Zhao, D. (2013). Bringing the ocean into the laboratory to probe the chemical complexity of sea spray aerosol. *Proceedings of the National Academy of Sciences of the United States of America*, *110*(19), 7550–7555. https://doi.org/10.1073/pnas.1300262110

Sampath, K., Afshar-Mohajer, N., Chandrala, L. D., Heo, W.-S., Gilbert, J., Austin, D., & Katz, J. (2019). Aerosolization of crude oil-dispersant slicks due to bubble bursting. *Journal of Geophysical Research: Atmospheres*, *124*(10), 5555–5578. https://doi.org/10.1029/2018JD029338

Sellegri, K., O'Dowd, C. D., Yoon, Y. J., Jennings, S. G., & de Leeuw, G. (2006). Surfactants and Submicron sea spray generation. *Journal of Geophysical Research*, *111*(D22). https://doi.org/10.1029/2005JD006658

Spiel, D. E. (1994). The number and size of jet drops produced by air bubbles bursting on a fresh water surface. *Journal of Geophysical Research: Oceans*, *99*(C5), 10289–10296. https://doi.org/10.3402/tellusb.v46i4.15808

Spiel, D. E. (1997). More on the births of jet drops from bubbles bursting on seawater surfaces. *Journal of Geophysical Research*, *102*(C3), 5815–5821. https://doi.org/10.1029/94JC03055

Veron, F. (2015). Ocean spray. *Annual Review of Fluid Mechanics*, *47*, 507–538.

Wang, X., Deane, G. B., Moore, K. A., Ryder, O. S., Stokes, M. D., Beall, C. M., & Prather, K. A. (2017). The role of jet and film drops in controlling the mixing state of submicron sea spray aerosol particles. *Proceedings of the National Academy of Sciences of the United States of America*, *114*(27), 6978–6983. https://doi.org/10.1073/pnas.1702420114

Woodcock, A. H., Kientzler, C. F., Arons, A. B., & Blanchard, D. C. (1953). Giant condensation nuclei from bursting bubbles. *Nature*, *172*(4390), 1144–1145. https://doi.org/10.1038/1721144a0

Yang, Y. M. & Maa, J. R. (1984). Bubble coalescence in dilute surfactant solutions. *Journal of Colloid and Interface Science*, *98*(1), 120–125. https://doi.org/10.1016/0021-9797(84)90484-3

References From the Supporting Information

Erinin, M. A., Wang, S. D., Liu, R., Towle, D., Liu, X., & Duncan, J. H. (2019). Spray generation by a plunging breaker. *Geophysical Research Letters*, *46*(14), 8244–8251. https://doi.org/10.1029/2019GL082831

Guildenbecher, D. R., Gao, J., Reu, P. L., & Chen, J. (2013). Digital holography simulations and experiments to quantify the accuracy of 3D particle location and 2D sizing using a proposed hybrid method. *Applied Optics*, *52*(16), 3790. https://doi.org/10.1364/AO.52.003790

Katz, J., & Sheng, J. (2010). Applications of holography in fluid mechanics and particle dynamics. *Annual Review of Fluid Mechanics*, *42*, 531–555. https://doi.org/10.1146/annurev-fluid-121108-145508